Piezoresistive response of extruded polyaniline/(styrene-butadiene-styrene) polymer blends for force and deformation sensors

J.Teixeira[1], L. Horta-Romarís [2], M.-J. Abad[2], P. Costa[1,3*], S. Lanceros-Mendez[4,5]

[1]Center of Physics, University of Minho, Campus de Gualtar, Braga, Portugal
[2]Universidade da Coruña, Grupo de Polímeros, Centro de Investigacións Tecnolóxicas, Campus de Esteiro, Ferrol, Spain
[3]Institute for Polymers and Composites IPC/I3N, University of Minho, 4800-058 Guimarães, Portugal
[4]BCMaterials, Parque Científico y Tecnológico de Bizkaia, Derio, Spain
[5]IKERBASQUE, Basque Foundation for Science, 48013 Bilbao, Spain

*Corresponding author. E-mail addresses: pcosta@fisica.uminho.pt

Abstract

Smart materials for sensor applications are increasingly being used in a wide variety of applications ranging from engineering to medical devices. This work reports on piezoresistive sensors based on conductive polyaniline and thermoplastic elastomer processed by conventional polymer extrusion. The material presents excellent processability and piezoresistive performance offering an alternative to traditional composites with conductive nanofillers for sensor applications. The polyaniline/ styrene-butadiene-styrene (PANI/SBS) conductive polymer blends present good mechanical properties, high electrical conductivity and piezoresistive response. The maximum strain reaches ≈60% for 30 weight percentage (wt%) PANI content and the electrical conductivity is σ ≈0.1 S/m for blends with 40 wt% PANI content. Further, the sample with 40 wt% PANI content shows a piezoresistive gauge factor GF ≈1 for deformation measurements between 0.1 to 3 mm in bending cycles.

Keywords: Polymer-matrix composites; Smart materials; Electrical properties; Piezoresistive; Extrusion

1. Introduction

Materials with piezoresistive properties represent a key engineering technology for device applications, being commonly used in industry and consumer products with ever growing demand [1-3]. Pressure or strain moldable sensors must be low profile and flexible to conform to arbitrary surfaces [4].

Most of the commercial piezoresistive sensors used in industrial applications are based on metallic films characterized by low flexibility and stretchability, limiting their range of applications [2, 5]. Semiconductor materials show high piezoresistive sensitivity but poor mechanical properties [1, 4]. In order to overcome these mechanical limitations, polymer-based smart materials have been developed due to their flexibility, low temperature processability and low cost [2, 6]. Further, these materials show simpler device integration and allow tailoring their overall physico-chemical properties for specific applications. Their outstanding properties result in a broad spectrum of engineering materials [5, 7] for sensors and actuators [8, 9], optoelectronics [10], low weight structures [11], antistatic dissipation [11] and dielectric devices [12], among others.

Promising applications of these materials are related to strain sensing technology for structural health monitoring and biomedical applications [4, 13]. Polymer composites with specific conductive characteristics can be developed using different materials (polymers and fillers) and strategies (processing methods and conditions). Extrinsically conducting polymers (ECPs) are based on conductive nanoparticles embedded in insulating polymer matrices. The most used conductive nanofillers are mostly based on carbonaceous materials, including carbon black, carbon nanofibers or nanotubes and graphene [7, 14]. The electrical conductivity of polymer composites as a function of filler content is characterized by different well-defined zones. The zone showing a strong increase of the electrical conductivity is identified as the percolation threshold (PT) and

strongly depends on the filler type and the composite processing method [15]. Thus, the PT can be as low as 0.01 wt% [15] for composites prepared by solvent casting or between 1 to 3 wt% for composites based on polymers with carbon nanotubes (CNT) processed with industrially viable methods such as melt compounding and extrusion [16]. Therefore, up scaled industrial processing for composite preparation typically lead to an increase of carbonaceous nanofiller loading content for achieving similar electrical properties when compared with laboratory methods.

In addition to ECPs, intrinsically conducting polymers (ICPs) also show piezoresistive properties and can be considered regarded a suitable alternative in terms of electrical conductivity and piezoresistive behavior response. Polyaniline, poly(3,4-ethylenedioxythiophene) (PEDOT), PEDOT modified with polystyrenesulfonate acid (PEDOT/PSS) and polypyrrole (PPy) [5] are examples of ICPs. These types of polymers can be used as piezoresistive sensors. In this way, the piezoresistive behavior of ICPs opens a new concept for piezoresistive sensors applications [17] but, on the other hand, ICPs present several limitations that need to be overcome. In particular with respect to their mechanical properties and longtime stability of the ICPs [17]. From the many available ICPs, polyaniline (PANI) has been implemented in a wide variety of applications, including biosensors [18], anti-static materials [19] and batteries [20], among others. PANI shows easy processing, low cost and stability, allied to the doping/dedoping mechanism, allowing to further tune material physico-chemical properties, makes the PANI one of the most interesting ICPs [5, 17].

Further, stretchable conductive composites are growing attention to replace the traditional rigid conductor materials, due to their applicability in flexible and stretchable devices [21]. Elastomer or thermoplastic elastomers (TPEs) polymer matrices are interesting materials in this context. TPEs are an important class of polymers that combine the mechanical properties of rubbers (e.g.,

stretchable materials) with the processability and recyclability of thermoplastics [22]. Additionally TPEs do not need vulcanization [6]. Styrene-butadiene-styrene (SBS) tri-block copolymer is an interesting TPE for the development of stress/strain sensors for large strain, robotic and industrial automation applications in order to replace silicone-like materials that are not capable of sustaining large deformations and sudden impacts [6]. Since SBS can be processed without the use of vulcanization, the properties of the corresponding composites do not deteriorate during their processing in composite materials [15]. With respect to the thermal behaviour, SBS has two T_g at -86 and 76 °C, assigned to the glass transitions of polybutadiene and polystyrene, respectively [22, 23].

In fact SBS and (styrene-ethylene/butylene-styrene) SEBS composites with CNT have been prepared by several methods, including solvent casting, electrospinning [24] and extrusion [15]. The different processing methods allow to prepare composites with excellent piezoresistive properties with gauge factors (GF) up to ≈120 and deformation up to 30% under uniaxial stress [8]. Elastomeric polymer composite with piezoresistive properties can be processed using other conductive carbon nanofillers such as graphene or carbon black within different rubber-like materials [25, 26]. Natural rubber/CNT composites show linear behaviour with mechanical stress for strains up to 250%, unlike graphene composites for lower strains [25]. The main drawback of composites with nanocarbonaceous fillers is the agglomeration of the nanofillers, which can be up to tens of micrometres in size [27, 28]. Another issue with respect to polymer composites is their poor adhesion of the polymer to fibre surfaces, being necessary the use of supplementary binders, which increase price and decrease electrical conductivity [29]. The agglomerates are defective structures that reduce the electrical and mechanical properties of the composite, leading to difficult reproducibility of the properties of the materials under the same manufacturing conditions. Further,

the presence of large nanofiller agglomerates hinders the use of specific sensors integration processes, such as printing techniques [30, 31].

Thus, PANI/TPE blends are an interesting alternative to polymer-based composites with conductive nanocarbonaceous fillers, due increased compatibility between the conductive polymer and the polymer matrix [32]. Further, the polymer blend can be processed by extrusion that, when compared to solvent-casting, commonly used for the preparation of piezoresistive polymer composites [15], has the advantage of being a purely mechanical process for polymer mixing which does not rely on the use of any chemical solvent. Further, it is a continuous process and allows the moulding of the resultant products.

The present work reports on extruded blend composites based on intrinsic conductive PANI embedded one a thermoplastic elastomer (SBS). The morphologic, electrical, mechanical and electromechanical properties of the PANI/SBS blends are reported as a function of PANI and compatibilizer content.

2. Experimental

2.1 Material synthesis

Aniline and potassium peroxodisulfate (APS) were purchased from Fluka (Steinheim, Germany). Dodecylbenzensulfonic acid (DBSA) 70 wt% solution in 2-propanol and acetone were obtained from Scharlau (Sentmenat, Spain). Chloroform and methanol were supplied from Merck (Darmstadt, Germany) and Octyl Gallate (OG) compatibilizer was acquired on Sigma-Aldrich (Madrid, Spain). All the solvents and reagents except DBSA were at least of 99% purity. Water was purified on a Milli-QUltrapure 109 system (Millipore, Molsheim, France).

Thermoplastic elastomer (TPE) copolymer based in styrene-butadiene-styrene (SBS) with reference Calprene 718 (75/25 butadiene/styrene ratio with a radial structure) was provided by Dynasol.

2.2 Processing of the conductive polymer and the polymer blend

Polyaniline (PANI-DBSA) was processed via indirect route with "dedoping-redoping" steps, as detailed in [19]. A doped polymer of hydrochloric acid, PANI-HCl, was subjected to two processing steps before obtaining a polymerized PANI-DBSA polymer according to the method described in [33].

1) PANI-HCl was dedoped with a solution of NH_3 (1M) for 2h in an ultrasonic bath. Then, the obtained solution was filtered under vacuum and washed with distilled water until a neutral pH was reached.
2) The filtrate was then subjected to doping with DBSA (1M) in acetone, being in ultrasonic bath for two hours. Acetone was also used to remove the excess of free acids on the solutions. Finally, the doped PANI-DBSA was filtered under vacuum and freeze-dried for 24h.

The polymer blends were processed by mixing PANI-DBSA with different quantities of powdered OG compatibilizer, ranging from 5 to 20%, and SBS in a Thermo Scientific Haake minilab II mini extruder at 150 °C for 15 minutes, followed by the extrusion of the blended mixture. The blend was then pressed in an IQAP-LAP model PL-15 hydraulic press for 6 minutes at 150 ºC, resulting in polymeric plates with an average thickness between 0.5 and 1 mm.

The OG compatibilizer, which presents an alkyl chain almost identical to DBSA, was selected in order to improve the solubility and conductivity of the blends [34].

A nomenclature presented in Table 1 was adopted for the PANI/SBS samples for an easier understanding during the presentation and discussion of the results. Samples with 20 and 30 wt% PANI content were processed, however these samples were not conductive, and they were just studied in terms of their mechanical properties.

Table 1- Nomenclature of the PANI/SBS blends.

PANI/SBS blend	Sample
20 wt% PANI/5 wt% OG/75 wt% SBS	PANI(20)/SBS(75)
30 wt% PANI/5 wt% OG/65 wt% SBS	PANI(30)/SBS(65)
40 wt% PANI/5 wt% OG/55 wt% SBS	PANI(40)/SBS(55)
40 wt% PANI/10 wt% OG/50 wt% SBS	PANI(40)/SBS(50)
40 wt% PANI/ 15 wt% OG/45 wt% SBS	PANI(40)/SBS(45)
40 wt% PANI/20 wt% OG/40 wt% SBS	PANI(40)/SBS(40)

2.3 Characterization of the materials

Polymer morphology was evaluated using Scanning Electron Microscopy (SEM). The images were obtained using a *JEOL JSM-6400* scanning electron microscope at an accelerating voltage of 20 kV with magnifications at 1000×, 3000× and 5000×.

Fourier transform infrared spectroscopy in the attenuated total reflection (FTIR-ATR) mode was performed in a *Jasco FT/IR-4700 FTIR spectra* spectrophotometer in the spectral range 4000 to 600 cm^{-1} with 100 interferograms at a spectral resolution of 4 cm^{-1}.

The thermal behaviour of the samples was evaluated by thermogravimetric analysis (TGA) using a *Perkin-Elmer TGA-7* set-up. The tests were carried out under oxygen atmosphere from 45°C to 700°C at a rate of 10 ºC/min. For each sample, the degradation temperature (T_{onset}), calculated as the extrapolated onset temperature in the TGA curve, and the temperature of the maximum degradation rate (T_{max}), measured as the first derivative peak temperature, were recorded.

Mechanical tests were performed with a universal testing machine (Shimadzu model AG-IS) at room temperature with a load cell of 50 N in tensile mode. The stress-strain characteristic curves were obtained under uniaxial stress applied from the upper clamp whereas the bottom clamp remained fixed. Rectangular shape samples with 10 x 6 mm^2 and 0.5 to 1 mm thickness (Fischer Dualscope 603-478, digital micrometer) were analyzed at a test velocity of 1 mm/min until rupture. Three measurements were performed for each sample.

The electrical conductivity of the samples was measured with a Keithley 487 picoammeter/voltage source. The current-voltage characteristic response was obtained in direct current (DC) mode with an applied voltage ranging between -10 V to 10 V, at room temperature. On each sample, two gold electrodes with diameter of 5 mm were deposited by magnetron sputtering on both sides of the samples using a SC502 sputter coater. The electrical conductivity (σ) was calculated by:

$$\sigma = \frac{1}{\rho} = \frac{1}{R}\frac{t}{A} \quad (1)$$

where R is the electrical resistance of the sample, A is the area of the electrodes and t is the thickness of the samples.

The piezoresistive properties of the PANI/SBS composites were evaluated by 4-point-bending tests (Figure 1) in which the electrical resistance variations were measured (Agilent 344401A multimeter) during loading-unloading mechanical cycles.

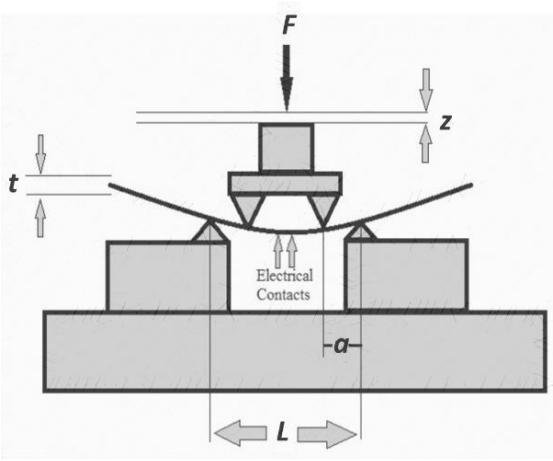

Figure 1- Schematic representation of the 4-point bending tests where *z* is the vertical displacement, *t* is the sample thickness, *a* is the distance between the first and second bending points and *L* the distance between the supports [22]. In the experimental tests, *a*=15 mm and *L*=3*a*.

The electrical resistance variations due to the mechanical deformation applied to the samples is quantitatively represented by the gauge factor (GF):

$$GF = \frac{\Delta R/R_0}{\varepsilon} \tag{2}$$

where ΔR and R_0 are the resistance variation and the initial resistance, respectively, and ε is the applied strain. The piezoresistive sensitivity of the materials has contributions from the intrinsic and the geometrical piezoresistive effect [1]. In the 4-point-bending measurements, the strain (ε) was calculated from the pure bending of plates theory, valid between the inner loading points and can be rewritten as [8]:

$$\varepsilon = \frac{3dz}{5a^2} \tag{3}$$

where *t* is the sample thickness, *z* is the deformation over time and *a* is the distance between the first and second pins of the 4-point bend load cell [8].

3. Results and Discussion

3.1. Morphological Properties

The morphology of the PANI/SBS extruded blends can be observed in the surface SEM images presented in Figure 1. Two magnifications are presented for each blend with 40 wt% PANI, 1000x and 5000x in order to evaluate the distribution of PANI within the polymer matrix.

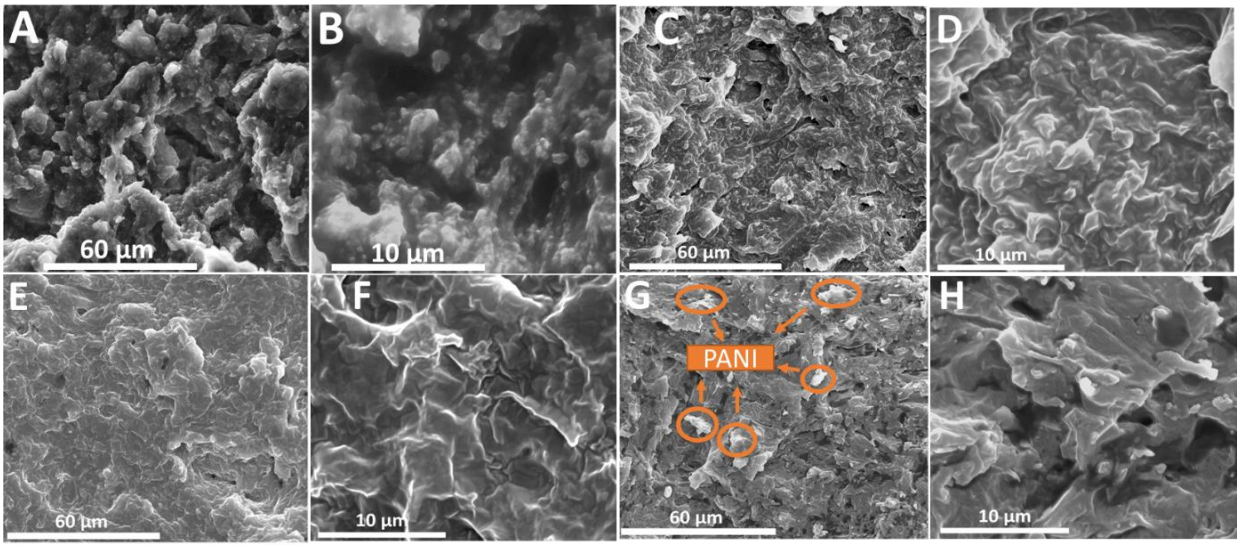

Figure 2- Surface SEM images of the PANI/SBS blends at two magnifications (1000x and 5000x, respectively) for A and B) PANI(40)/SBS(55), C and D) PANI(40)/SBS(50), E and F) PANI(40)/SBS(45) and G and H) PANI(40)/SBS(40) blends.

The morphology of the PANI/SBS blends with 40 wt% PANI content and SBS content ranging from 40 to 55 wt%, is shown in Figure 2. The SEM images are representative for the remaining

blends. All samples show good dispersion of the PANI within the SBS matrix, showing just small aggregates of few micrometer in diameter. The indirect synthesis of PANI with DBSA is environment-friendly, as it avoids chloroform during processing, and the obtained PANI particles are nanorods, allowing a good dispersion within the polymer matrix [19]. Further, the elongated shape of the PANI/DBSA particles improves the electrical conductivity of both PANI and the corresponding composites, when compared to other synthesis procedures and dopants [19]. Further, Figure 2 shows a good compatibilization between PANI and SBS, independently of the PANI, OG or SBS relative content of the different blends.

FTIR spectra of doped PANI-DBSA and PANI/SBS blends are presented in Figure 3. The characteristic bands of the PANI-DBSA are the Quinoid (Q) and Benzenoid (B) that appear at 1558 and 1450 cm^{-1}. For the SBS matrix, the characteristic polystyrene and polybutadiene bands are located at 696 and 963 cm^{-1}, respectively.

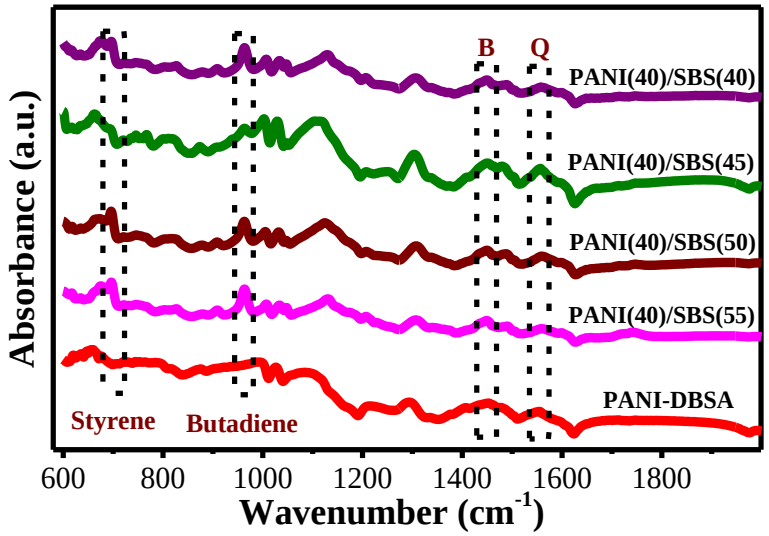

Figure 3- FTIR spectra from 600 to 2000 cm^{-1} for PANI-DBSA and PANI/SBS blends with 40 wt% of PANI and different SBS contents (from 40 to 55 wt%). The typical Benzenoid (B) and Quinoid (Q) bands of PANI and the polystyrene and polybutadiene bands of SBS are identified.

PANI-DBSA shows the bands assigned to the Benzenoid (B, $\upsilon_{C=C}$) and Quinoid (Q, $\upsilon_{C=N}$, $\upsilon_{C=C}$) moieties at 1450 and 1558 cm^{-1}, respectively, as indicated in the literature [19, 35]. The ratio between these bands proves that the produced PANI-DBSA is in fact in the emeraldine state.

The intensity ratio between these two bands (I_Q/I_B) provides information on the molecular structure of the doped PANI. Typically, a value around 1 indicates that PANI is in its emeraldine type structure, which presents the highest electrical conductivity among the different PANI molecular structures [19]. The ratio between both intensities in PANI-DBSA and blends chages from 0.96 to 0.98, indicative of an emeraldine form [19].

3.2. Thermal Properties

The thermal behaviour of PANI, SBS, compatibilizer (OG) and blends is shown in Figure 4.

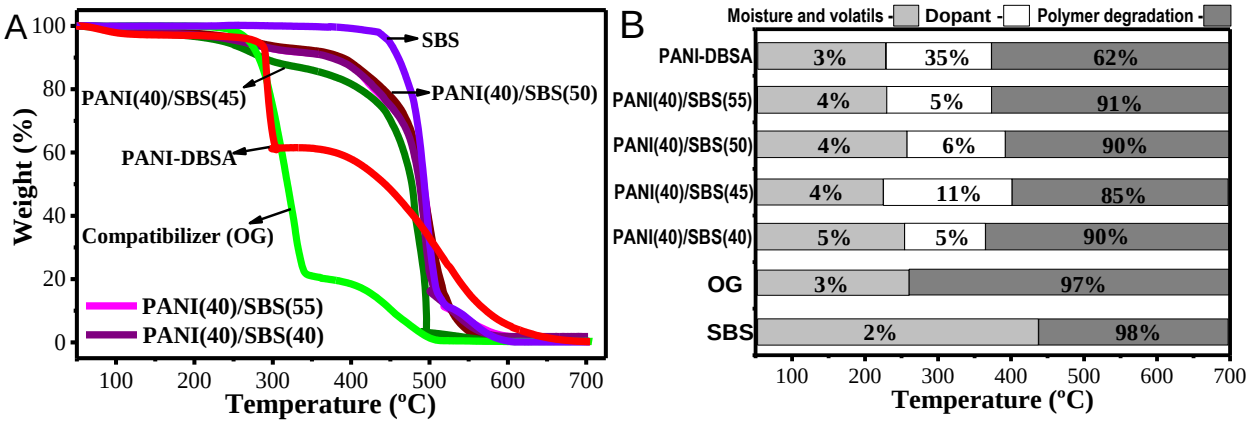

Figure 4- A) Thermogravimetric analysis of PANI-DBSA, OG, SBS and several PANI/SBS blends with varying the SBS contents from 40 to 55 wt%. Measurements performed at 10 ºC/min. B) Temperature intervals with corresponding weight losses for the different degradation (Moisture and volatiles, dopant and polymer degradation) events of different samples.

The elastomer SBS presents a thermal behavior with a degradation temperature, T_{onset}, around 435 ºC and a temperature of maximum degradation rate (T_{max}), around 500 ºC. T_{max} for blends is near 500 ºC. The OG has a T_{onset} near 250 ºC and T_{max} before 500 ºC (Figure 4A). Literature shows that doped PANI loses near 35 wt% around 300 ºC attributed to evaporation of absorbed water and organic solvent [36]. Further, complete degradation occurs after 600 ºC [19, 36], as observed in Figure 4. This main mass loss is assigned to decomposition of the doping agent DBSA and organic groups of PANI [19, 36]. In this way, the first derivative peak temperature (data not shown) close to 400 ºC is due PANI and OG, once SBS degradation (measured as T_{onset} or T_{max}) starts after this point [37].

All PANI/SBS blends present similar degradation behavior, independently of the SBS, OG and PANI relative contents in the blends. The first degradation step occurs around 250 ºC and the temperature of maximum degradation rate (T_{max}) is around 500 ºC. The PANI and OG contents in the blends influences the T_{onset} but the T_{max} is similar for the different blends and pure SBS. The initial degradation temperature of the OG and PANI is near 250 and 300 ºC [19, 36], respectively. The PANI/SBS blends with 40 wt% PANI and from 5 to 20 wt % of OG starts the degradation at lower temperature, when compared to SBS. However, the behavior is similar for the different blends. The blends show thermal stability up to near 400 ºC, losing less than 15% of their weight (Figure 4B).

Although the OG has lower degradation temperature, even in samples with larger OG contents, the thermal stability of the blends is independent of the OG amount, for 5 to 20 wt% (Figure 4B).

3.3. Mechanical Properties

The mechanical behaviour of the extruded PANI/SBS blends is presented in Figure 5 through the stress/strain characteristics. The Young modulus of the blends was obtained for deformations at 1% of strain.

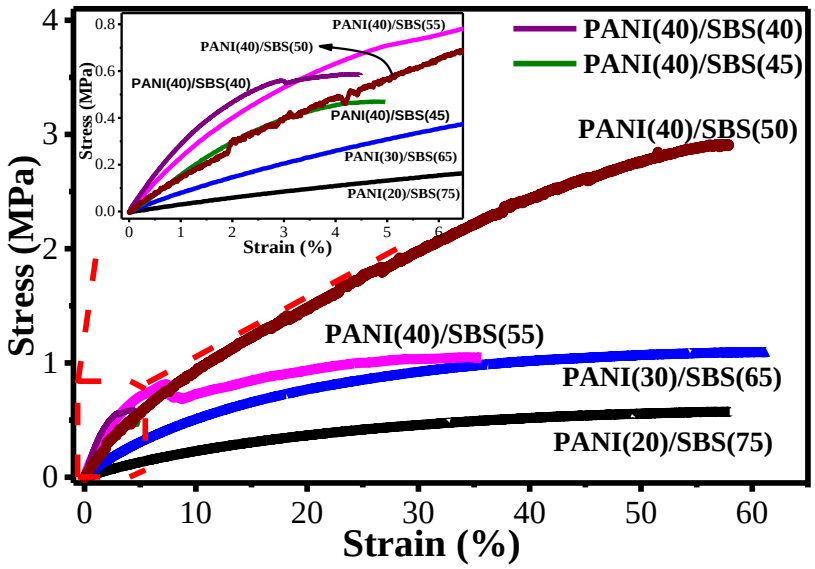

Figure 5- Stress-strain behavior of several PANI/SBS blends until rupture at deformation rates of 1 mm/min. The PANI content varies from 20 to 40 wt% and the SBS content from 40 to 75 wt%, ranging the OG from 5 to 20 wt%.

The PANI/SBS blends with increasing SBS content leads to samples with larger maximum strain and lower maximum stress. The maximum strain is around 60% for blends with higher SBS contents and around 5% for blends with lower SBS contents (Figure 5). It is to notice that extruded SBS shows maximum strains larger than 1000% and Young modulus around 1.5 MPa [15]. On the other hand, PANI shows low stretchability (around 5 to 6% of strain) and a higher Young modulus of few GPa [38, 39]. Thus, the polymer blends increase the stretchability of the conducting component (PANI), allowing the development of stretchable sensors applications. Further, both

PANI and the OG influences the mechanical properties of the blends. For samples with 40 wt% of PANI, the mechanical behavior of the blends suffer strong variations (essentially the maximum strain) with decreasing SBS and increasing OG content in the blends. The maximum strain decreases one order of magnitude from 55 wt% to 40 wt% content of SBS within the blends. There is no direct influence of the OG on the Young modulus of the blends, with an exception of the PANI(40)/SBS(40) which presents a higher Young modulus (~30 MPa).

Table 2 shows the main mechanical properties of the PANI/SBS composites obtained from the data in Figure 5.

Table 2- Main mechanical properties of the several extruded PANI/SBS blends.

Sample	Young Modulus (MPa)	Rupture Stress (%)	Rupture Strain (%)
PANI(40)/SBS(40)	30.5 ± 1.5	0.6 ± 0.1	4.4 ± 0.6
PANI(40)/SBS(45)	16.1 ± 0.5	0.5 ± 0.1	5.0 ± 0.7
PANI(40)/SBS(50)	15.0 ± 1.1	2.9 ± 0.2	57.9 ± 5
PANI(40)/SBS(55)	17.3 ± 1.0	1.1 ± 0.1	35.6 ± 4
PANI(30)/SBS(65)	7.7 ± 0.4	1.1 ± 0.1	61.4 ± 5
PANI(20)/SBS(75)	3.1 ± 0.16	0.6 ± 0.1	58.0 ± 4

Table 2 shows that the composition of the blends affects the overall mechanical properties. The Young modulus (measured up to 1% of strain) decreases from 30 to 3 MPa with increasing SBS and decreasing PANI content in the blends. Decreasing the PANI contents from 40 to 20 wt% leads to a decrease of the Young modulus of the blends in approximately one order of magnitude. The Young modulus increases one order of magnitude with decreasing the soft component, remaining far from the values of PANI.

Increasing the softer polymer within the blends increases their stretchability (rupture strain) from 4.5 to near 60%.

The Yield strain increases with increasing SBS contents, being near 1.4% for blends with lower SBS contents and increasing until 17% for blend with larger contents of SBS. Thus, SBS gives the stretchability to the extruded blends, being interesting for large strain devices applications.

The mechanical properties of the blends are influenced by the relative polymer content. The Young modulus is mainly influenced by the SBS content. On the other hand, with respect to the maximum strain, the PANI properties overlaps the ones from SBS, since the blend breaks though the PANI and OG components.

3.4. Electrical Properties

The electrical conductivity behavior of the PANI/SBS blends as a function of PANI and SBS contents is shown in Figure 6. The percolation threshold is between 20 and 30 wt% PANI content.

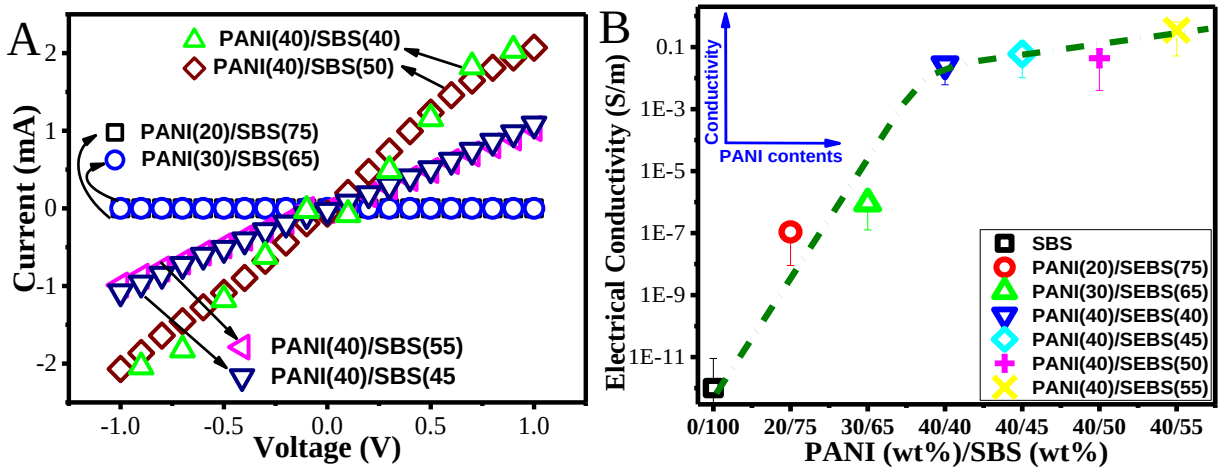

Figure 6- Electrical properties of the PANI/SBS blends with A) I-V curves between -1 to +1 V and B) conductivity of the PANI/SBS blends up to 40 wt% PANI. The electrical percolation threshold is around 20-30 wt% of PANI in the blends. The line in B) is for guiding the eyes.

The slope of the I-V curves (Figure 6A) increases with increasing PANI content (electrical conductive compound) in the blends, from 20 to 40 wt%. Thus, the electrical conductivity of the blends (Figure 6B) increases with increasing conductive polymer content, as doped PANI with DBSA has an electrical conductivity σ≈ 990 S/m [19]. The PANI/SBS blends shows an electrical conductivity that increases six orders of magnitude, varying from$1x10^{-7}$ S/m to ≈0.1 S/m for samples with 20 and 40 wt% PANI content in blend, respectively. PANI/SBS blends with 40 wt% PANI show similar electrical conductivity, being slightly higher for the sample with higher contents of SBS (and consequently lower contents of the OG). Thus, the electrical conductivity in the blend is basically determined by the PANI content. The electrical percolation threshold is between 20 to 30 wt% PANI content in the blends. Thus, it is shown that it is possible to develop thermoplastic PANI/elastomer blends with suitable conductivity and mechanical properties for sensors applications, using an industrial processing method.

PANI/SBS blends present larger percolation threshold when compared to composites with similar matrices but using conductive carbonaceous nanofillers such as carbon nanotubes. Extruded CNT/SBS composites present percolation thresholds between 4 and 5 wt% CNT [15], and, in composites prepared by solvent casting, the percolation threshold is much lower than for extruded composites [6, 8, 40]. Percolation threshold depends on the polymer matrix, conductive nanofiller type and processing method [40]. The highest electrical conductivity PANI/SBS blends with 40 wt% can be compared to the ones obtained for composites with different conductive nanofillers [40, 41]. In this way, extruded PANI/SBS blends can be excellent alternative polymer-based materials to conductive nanocomposites for specific electro-mechanical applications.

3.5. Electro-mechanical Properties

Analyzing the simultaneously the mechanical and electrical properties of the PANI/SBS blends, the piezoresistive response was evaluated for PANI(40)/SBS(55) blends in which the maximum strain is higher than 30% and the electrical conductivity is around 0.1 S/m. These blends also present lower OG contents, having lower influence in the piezoresistive response of the material. On the other hand, mechanical properties of the blends with lower SBS contents show low maximum deformation, compared to the remaining blends.. Further, the similar electrical conductivity between PANI(40)/SBS(50) and PANI(40)/SBS(55) makes the piezoresistive response of these blends very analogous. The piezoresistive response was evaluated as a function of deformation, stability with larger number of cycles and temperature (Figure 7 to 9).

Figure 7 illustrate the piezoresistive response of the PANI(40)/SBS(55) blend in 4-point-bending experiments for 0.1 and 3 mm of deformation (Figure 7A and B, respectively).

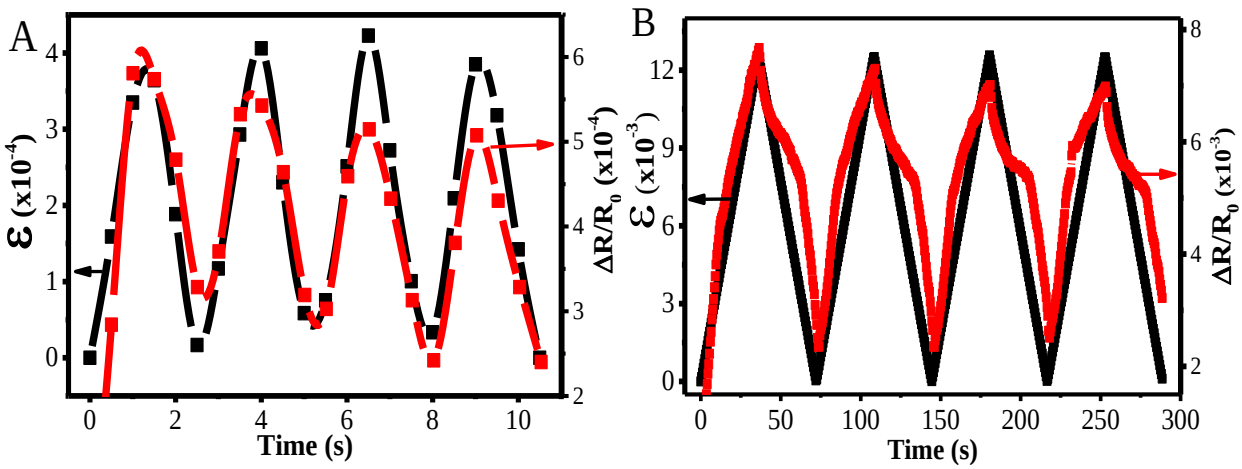

Figure 7- Piezoresistive response of PANI(40)/SBS(55) blends for A) 0.1 and B) 3 mm of deformation in 4-point-bending experiments. The electrical resistance variation follows the mechanical stimulus applied to the blends the different deformations.

Figures 7A and 7B show the piezoresistive behavior of the PANI(40)/SBS(55) blends, in 4-point-bending measurements for 0.1 and 3 mm of deformation, the response being similar for intermediate deformations of 0.5, 1 and 2 mm. This piezoresistive behavior is illustrative for the different PANI/SBS blends with different PANI content (above the percolation threshold) and deformations from 0.1 to 3%, all following a similar behavior for the electrical resistance variation with applied mechanical stimulus. The electrical resistance increases while the blend is deformed and decreases when the blend recovers to the initial deformation. The behavior is similar for all loading/unloading mechanical conditions. The gauge factor (GF) is determined by the linear variation of the electrical resistance with deformation (Equation 2) and exemplified in Figure 8A for several deformations (between 0.5 to 2 mm). Figure 8B shows the GF of the PANI(40)/SBS(55) blend as a function of the deformation.

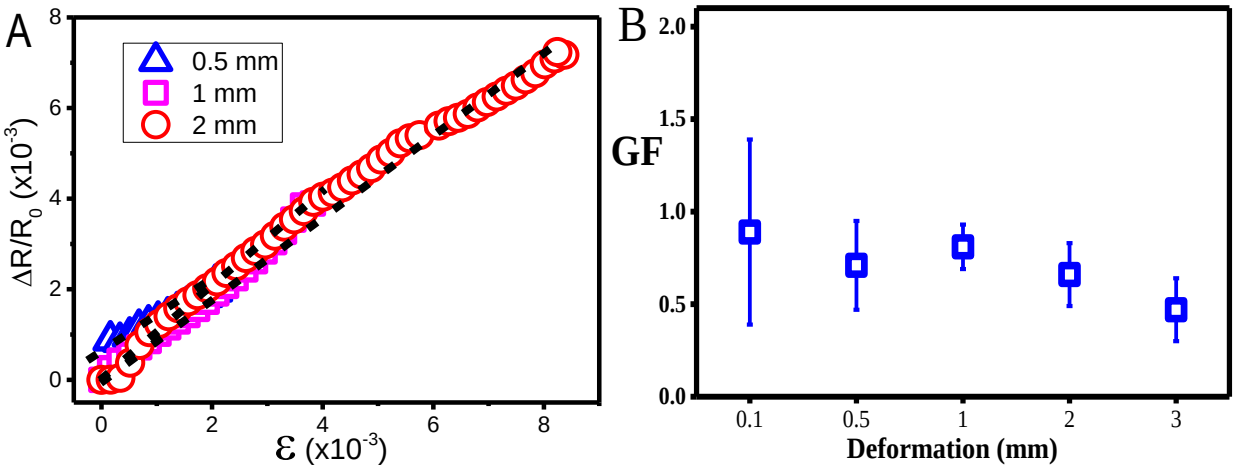

Figure 8- Piezoresistive sensitivity of the PANI/SBS blend with 40 wt% PANI and 55 wt% SBS) in 4-point-bending experiments from 0.1 to 3 mm of deformation. A) Determination of the Gauge Factor (GF) in each deformation cycle and B) GF as function of the applied maximum deformation.

The relative electrical resistance variation follows the applied mechanical cycles, increasing when the samples are deformed and decreasing when the blend relaxes to the initial position, as can be observed in Figure 7 and 8A.

The PANI(40)/SBS(55) blend present good piezoresistive response and PANI/SBS samples can be used as piezoresistive materials for sensors applications. The piezoresistive sensitivity of the PANI(40)/SBS(55) is presented in Figure 8B, showing a GF between 0.5 to 1 for deformations until 3 mm and the GF decreasing slightly with increasing deformation. Thus, the GF is mainly determined by the geometrical piezoresistive response ($1+2\nu$).

Considering the piezoresistive response of the PANI(40)/SBS(55) blend, experiments were performed as a function of the number of load/unload cycles (250) to evaluate the stability and fatigue of the PANI/SBS blend (data not shown). The electrical resistance shows slightly decrease (some few Ohms) in the initial cycles and tend to stabilize after the 10th deformation cycle. The GF, on the other hand, increases slightly with increase the number of cycles between GF ≈0.9 to 1.1 (Figure 9A). The GF stabilizes after ~120 cycles. Further, the piezoresistive response is stable in temperature up to temperatures of 40 ºC (Figure 9B).

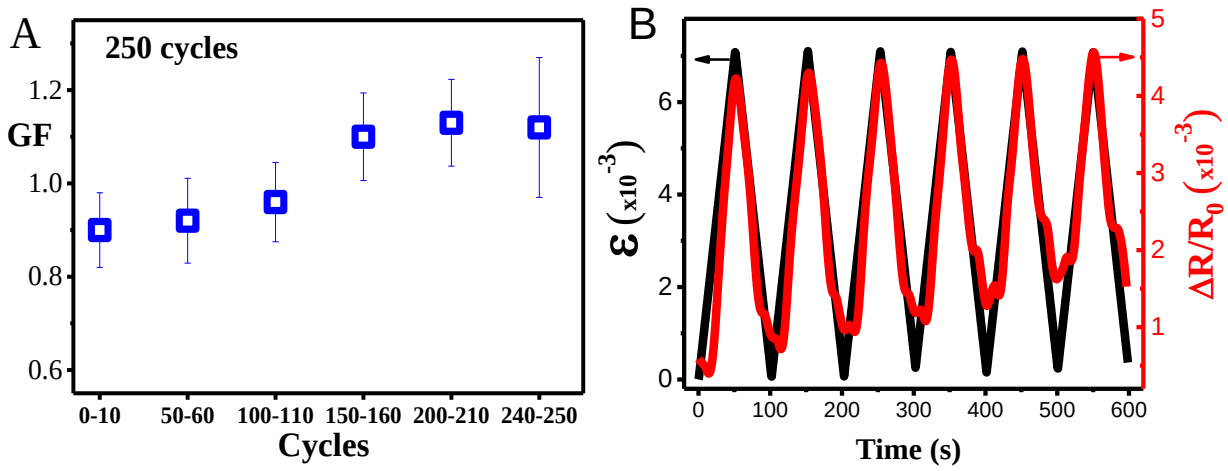

Figure 9- Piezoresistive sensitivity (GF) of the PANI/SBS blend with 40 wt% PANI and 55 wt% SBS, in 4-point-bending measures as a function of the number of cycles (A) Piezoresistive response at a temperature of 40 ºC(B).

Thus, PANI/SBS blends present stable piezoresistive response after few cycles proving their suitability for strain sensor applications. The increase of the piezoresistive sensibility, from GF≈ 0.9 to 1.1, with increasing number cycles reflects the larger electrical resistance variation after mechanical stabilization of the blend (release of internal stresses related to processing). Further, the piezoresistive response is stable up to 40 ºC, with a GF≈ 0.93 ±0.1, like the one observed at room temperature. For temperatures close to 60 ºC, the blend loses the piezoresistive response, essentially due to both, the glass transition (T_g≈ 75 ºC [15]) of the polystyrene chains in the SBS matrix, and the thermal degradation of PANI.

The piezoresistive sensitivity of the PANI/SBS blends is slightly lower compared to related polymer based composites prepared with conductive nanofillers [8, 15]. Polyaniline is characterized by a larger Young modulus, around 1 GPa [38, 42], when compared to SBS matrix, with a Young modulus between 50 to 100 MPa [22]. In this way, during mechanical deformation,

the PANI regions within the blend suffer inferior strain compared to the elastomeric SBS in blend. Thus, the piezoresistive sensitivity can be lower in this type of blends once the conductive network does not suffer same intrinsic variations of the electrical resistivity of PANI upon mechanical stretching, and the geometric effect dominates the piezoresistive sensitivity on PANI/SBS blends.

4. Conclusions

Extruded PANI/SBS blends offer an interesting alternative to conductive nanocarbonaceous/polymer piezoresistive composites. The processed blends have good mechanical and piezoresistive properties, as the extrusion method allows a good dispersion of the aggregates of PANI in the SBS polymer.

Deformations up to 60% in uniaxial stress are obtained before break for the PANI/SBS blends with the higher SBS contents. The electrical conductivity of the blends increases with increase conductive PANI content reaching a maximum conductivity of 0.1 S/m for the samples with 40 wt% PANI contents. Further, this sample shows a piezoresistive beinding response with a GF≈ 1, stable over repeated cycling and up to temperatures of 40 ºC, being suitable for sensor applications.

Acknowledgements

This work was supported by the Portuguese Foundation for Science and Technology (FCT) in the framework of the Strategic Funding UID/FIS/04650/2013. The authors thank the FCT for financial support under projects PTDC/EEI-SII/5582/2014 and PTDC/CTM-ENE/5387/2014. P. C. also thank the FCT for the SFRH/BPD/110914/2015 grant, as well POCH and European Union. Financial support from the Basque Government Industry Department under the ELKARTEK Program is also acknowledged as well as funding by the Spanish Ministry of Economy and

Competitiveness (MINECO) through the project MAT2016-76039-C4-3-R and by Xunta de Galicia-FEDER though the Program of Consolidation and structuring competitive research units (GRC2014/036)

References

[1] B.F. Gonçalves, J. Oliveira, P. Costa, V. Correia, P. Martins, G. Botelho, S. Lanceros-Mendez, Development of water-based printable piezoresistive sensors for large strain applications, Composites Part B: Engineering 112 (2017) 344-352.

[2] A.S. Zuruzi, T.M. Haffiz, D. Affidah, A. Amirul, A. Norfatriah, M.H. Nurmawati, Towards wearable pressure sensors using multiwall carbon nanotube/polydimethylsiloxane nanocomposite foams, Materials & Design 132(Supplement C) (2017) 449-458.

[3] T. Yang, D. Xie, Z. Li, H. Zhu, Recent advances in wearable tactile sensors: Materials, sensing mechanisms, and device performance, Materials Science and Engineering: R: Reports 115(Supplement C) (2017) 1-37.

[4] J. DeGraff, R. Liang, M.Q. Le, J.-F. Capsal, F. Ganet, P.-J. Cottinet, Printable low-cost and flexible carbon nanotube buckypaper motion sensors, Materials & Design 133(Supplement C) (2017) 47-53.

[5] E. Falletta, P. Costa, C. Della Pina, S. Lanceros-Mendez, Development of high sensitive polyaniline based piezoresistive films by conventional and green chemistry approaches, Sensors and Actuators A: Physical 220 (2014) 13-21.

[6] B.F. Gonçalves, P. Costa, J. Oliveira, S. Ribeiro, V. Correia, G. Botelho, S. Lanceros-Mendez, Green solvent approach for printable large deformation thermoplastic elastomer based piezoresistive sensors and their suitability for biomedical applications, Journal of Polymer Science, Part B: Polymer Physics 54(20) (2016) 2092-2103.

[7] T.K. Das, S. Prusty, Graphene-Based Polymer Composites and Their Applications, Polymer-Plastics Technology and Engineering 52(4) (2013) 319-331.

[8] P. Costa, A. Ferreira, V. Sencadas, J.C. Viana, S. Lanceros-Méndez, Electro-mechanical properties of triblock copolymer styrene–butadiene–styrene/carbon nanotube composites for large deformation sensor applications, Sensors and Actuators A: Physical 201 (2013) 458-467.

[9] N. Sahiner, S. Demirci, The use of graphene oxide-embedded superporous poly(2-hydroxyethylmethacrylate) cryogels for p(aniline) conductive polymer synthesis and their use in sensor applications, Materials & Design 120(Supplement C) (2017) 47-55.

[10] B. Pradhan, R.R. Kohlmeyer, K. Setyowati, H.A. Owen, J. Chen, Advanced carbon nanotube/polymer composite infrared sensors, Carbon 47(7) (2009) 1686-1692.

[11] O. Breuer, U. Sundararaj, Big returns from small fibers: A review of polymer/carbon nanotube composites, Polymer Composites 25(6) (2004) 630-645.

[12] K. Tsuchiya, A. Sakai, T. Nagaoka, K. Uchida, T. Furukawa, H. Yajima, High electrical performance of carbon nanotubes/rubber composites with low percolation threshold prepared with a rotation-revolution mixing technique, Composites Science and Technology 71(8) (2011) 1098-1104.

[13] T. Del Castillo-Castro, M.M. Castillo-Ortega, P.J. Herrera-Franco, Electrical, mechanical and piezo-resistive behavior of a polyaniline/poly(n-butyl methacrylate) composite, Composites Part A: Applied Science and Manufacturing 40(10) (2009) 1573-1579.

[14] S. Stankovich, D.A. Dikin, G.H.B. Dommett, K.M. Kohlhaas, E.J. Zimney, E.A. Stach, R.D. Piner, S.T. Nguyen, R.S. Ruoff, Graphene-based composite materials, Nature 442(7100) (2006) 282-286.

[15] P. Costa, C. Silvia, J.C. Viana, S. Lanceros Mendez, Extruded thermoplastic elastomers styrene–butadiene–styrene/carbon nanotubes composites for strain sensor applications, Composites Part B: Engineering 57 (2014) 242-249.

[16] E. Bilotti, H. Zhang, H. Deng, R. Zhang, Q. Fu, T. Peijs, Controlling the dynamic percolation of carbon nanotube based conductive polymer composites by addition of secondary nanofillers: The effect on electrical conductivity and tuneable sensing behaviour, Composites Science and Technology 74 (2013) 85-90.

[17] S. Bhadra, D. Khastgir, N.K. Singha, J.H. Lee, Progress in preparation, processing and applications of polyaniline, Progress in Polymer Science 34(8) (2009) 783-810.

[18] C. Dhand, M. Das, M. Datta, B.D. Malhotra, Recent advances in polyaniline based biosensors, Biosensors and Bioelectronics 26(6) (2011) 2811-2821.

[19] L. Horta-Romarís, M.-J. Abad, M.V. González-Rodríguez, A. Lasagabáster, P. Costa, S. Lanceros-Méndez, Cyclic temperature dependence of electrical conductivity in polyanilines as a function of the dopant and synthesis method, Materials & Design 114 (2017) 288-296.

[20] F. Cheng, W. Tang, C. Li, J. Chen, H. Liu, P. Shen, S. Dou, Conducting Poly(aniline) Nanotubes and Nanofibers: Controlled Synthesis and Application in Lithium/Poly(aniline) Rechargeable Batteries, Chemistry – A European Journal 12(11) (2006) 3082-3088.

[21] Y. Luan, J.-S. Noh, S.H. Kim, Facile control of stretchability and electrical resistance of elastomer/polyaniline composites for stretchable conductors, Materials Chemistry and Physics 190 (2017) 68-73.

[22] P. Costa, J. Silva, V. Sencadas, R. Simoes, J.C. Viana, S. Lanceros-Méndez, Mechanical, electrical and electro-mechanical properties of thermoplastic elastomer styrene–butadiene–styrene/multiwall carbon nanotubes composites, Journal of Materials Science 48(3) (2013) 1172-1179.

[23] R.-S. Shih, S.-W. Kuo, F.-C. Chang, Thermal and mechanical properties of microcellular thermoplastic SBS/PS/SBR blend: effect of crosslinking, Polymer 52(3) (2011) 752-759.

[24] S. Ribeiro, P. Costa, C. Ribeiro, V. Sencadas, G. Botelho, S. Lanceros-Méndez, Electrospun styrene–butadiene–styrene elastomer copolymers for tissue engineering applications: Effect of butadiene/styrene ratio, block structure, hydrogenation and carbon nanotube loading on physical properties and cytotoxicity, Composites Part B: Engineering 67 (2014) 30-38.

[25] H. Aguilar-Bolados, M. Yazdani-Pedram, A. Contreras-Cid, M.A. López-Manchado, A. May-Pat, F. Avilés, Influence of the morphology of carbon nanostructures on the piezoresistivity of hybrid natural rubber nanocomposites, Composites Part B: Engineering 109 (2017) 147-154.

[26] Y. Huang, X. He, L. Gao, Y. Wang, C. Liu, P. Liu, Pressure-sensitive carbon black/graphene nanoplatelets-silicone rubber hybrid conductive composites based on a three-dimensional polydopamine-modified polyurethane sponge, Journal of Materials Science: Materials in Electronics (2017) 1-10.

[27] L.C. Herrera-Ramírez, P. Castell, J.P. Fernández-Blázquez, Á. Fernández, R. Guzmán de Villoria, How do graphite nanoplates affect the fracture toughness of polypropylene composites?, Composites Science and Technology 111 (2015) 9-16.

[28] X. Zhao, J. Zhao, J.-P. Cao, D. Wang, G.-H. Hu, F. Chen, Z.-M. Dang, Effect of the selective localization of carbon nanotubes in polystyrene/poly(vinylidene fluoride) blends on their dielectric, thermal, and mechanical properties, Materials & Design (1980-2015) 56(Supplement C) (2014) 807-815.

[29] M. Zahid, E.L. Papadopoulou, A. Athanassiou, I.S. Bayer, Strain-responsive mercerized conductive cotton fabrics based on PEDOT:PSS/graphene, Materials & Design 135(Supplement C) (2017) 213-222.

[30] P. Mellin, C. Jönsson, M. Åkermo, P. Fernberg, E. Nordenberg, H. Brodin, A. Strondl, Nano-sized by-products from metal 3D printing, composite manufacturing and fabric production, Journal of Cleaner Production 139 (2016) 1224-1233.

[31] J.F. Christ, N. Aliheidari, A. Ameli, P. Pötschke, 3D printed highly elastic strain sensors of multiwalled carbon nanotube/thermoplastic polyurethane nanocomposites, Materials & Design 131(Supplement C) (2017) 394-401.

[32] F.X. Perrin, C. Oueiny, Polyaniline thermoset blends and composites, Reactive and Functional Polymers 114 (2017) 86-103.

[33] P. Saini, R. Jalan, S.K. Dhawan, Synthesis and characterization of processable polyaniline doped with novel dopant NaSIPA, Journal of Applied Polymer Science 108(3) (2008) 1437-1446.

[34] M.S. Dopico-García, A. Ares, A. Lasagabáster-Latorre, X. García, L. Arboleda, M.J. Abad, Extruded polyaniline/EVA blends: Enhancing electrical conductivity using gallate compatibilizers, Synthetic Metals 189 (2014) 193-202.

[35] V. Kumar, T. Yokozeki, T. Goto, T. Takahashi, Synthesis and characterization of PANI-DBSA/DVB composite using roll-milled PANI-DBSA complex, Polymer 86 (2016) 129-137.

[36] S. Xiong, S. Li, X. Zhang, R. Wang, R. Zhang, X. Wang, B. Wu, M. Gong, J. Chu, Synthesis and Performance of Highly Stable Star-Shaped Polyaniline Electrochromic Materials with Triphenylamine Core, Journal of Electronic Materials (2017).

[37] C. Direksilp, P. Threepopnatkul, Performance Improvement of PS from Expanded Polystyrene Off-grade, Energy Procedia 56 (2014) 135-141.

[38] H. Valentová, J. Stejskal, Mechanical properties of polyaniline, Synthetic Metals 160(7–8) (2010) 832-834.

[39] K.-Y. Shin, M. Kim, J.S. Lee, J. Jang, Highly Omnidirectional and Frequency Controllable Carbon/Polyaniline-based 2D and 3D Monopole Antenna, Scientific Reports 5 (2015) 13615.

[40] K.K. Sadasivuni, D. Ponnamma, S. Thomas, Y. Grohens, Evolution from graphite to graphene elastomer composites, Progress in Polymer Science 39(4) (2014) 749-780.

[41] H. Deng, L. Lin, M. Ji, S. Zhang, M. Yang, Q. Fu, Progress on the morphological control of conductive network in conductive polymer composites and the use as electroactive multifunctional materials, Progress in Polymer Science 39(4) (2014) 627-655.

[42] S.J. Pomfret, P.N. Adams, N.P. Comfort, A.P. Monkman, Electrical and mechanical properties of polyaniline fibres produced by a one-step wet spinning process, Polymer 41(6) (2000) 2265-2269.

Graphical Abstract

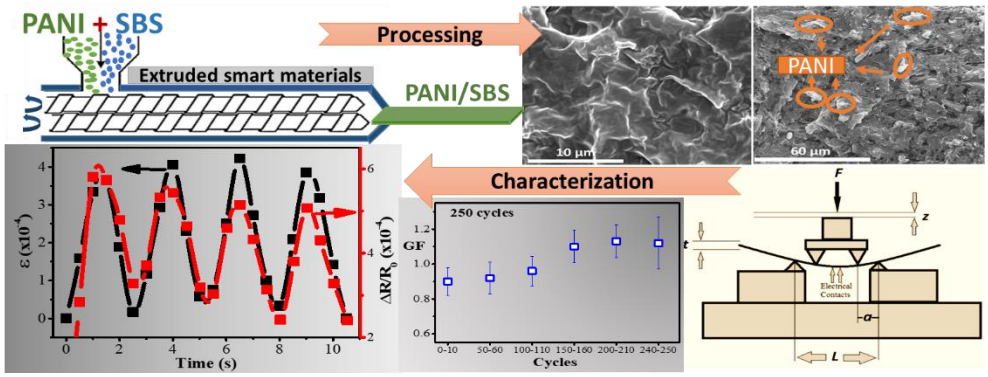

Figures

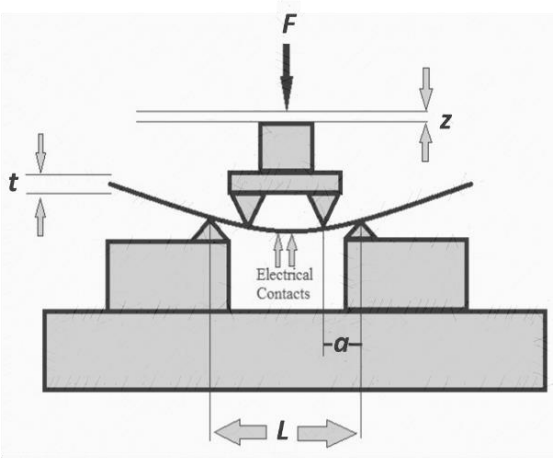

Figure 1- Schematic representation of the 4-point bending tests where *z* is the vertical displacement, *t* is the sample thickness, *a* the distance between the first and second bending points and *L* the distance between the supports [29]. In the experimental tests, *a*=15 mm and *L*=3a.

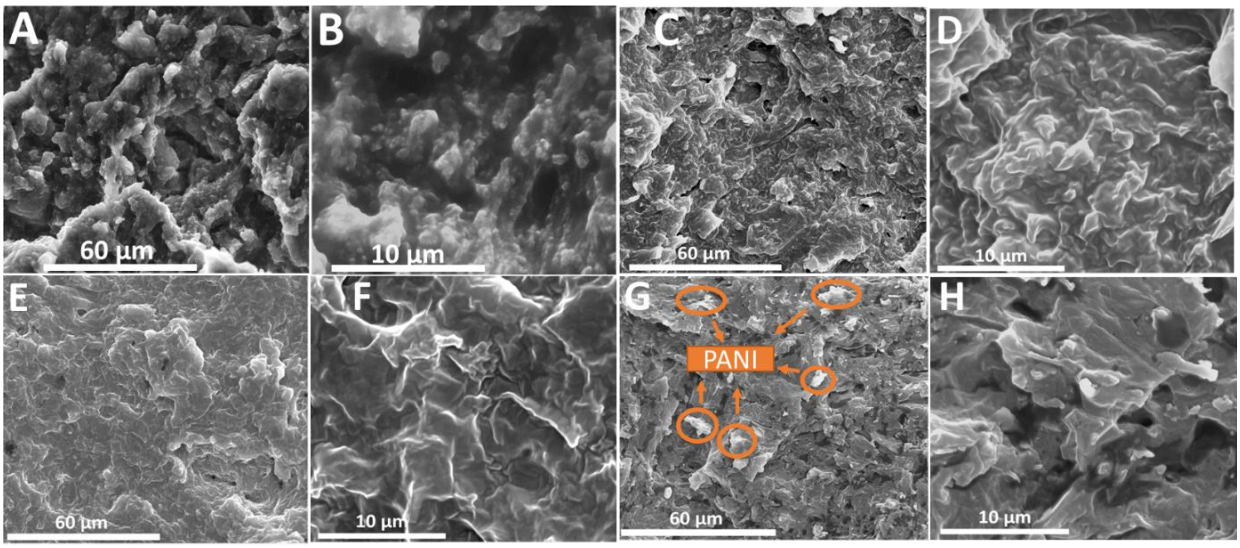

Figure 10- Surface SEM images of the PANI/SBS blends at two magnifications (1000x and 5000x, respectively) for A and B) PANI(40)/SBS(55), C and D) PANI(40)/SBS(50), E and F) PANI(40)/SBS(45) and G and H) PANI(40)/SBS(40) blends.

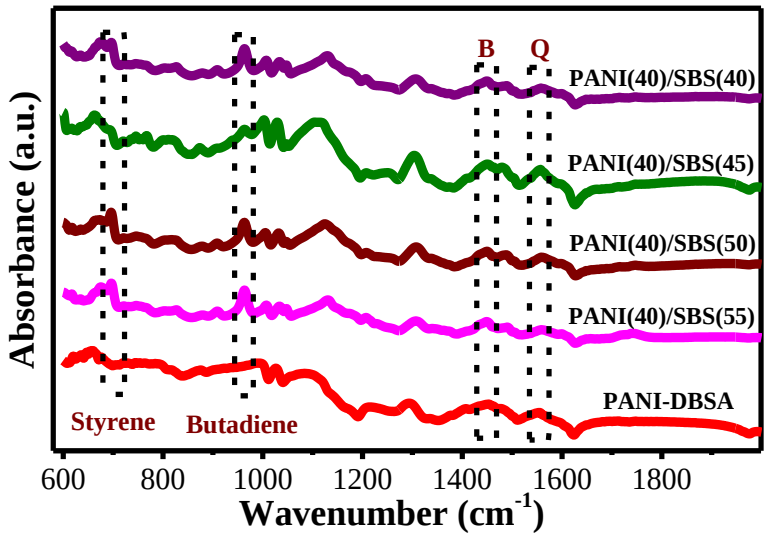

Figure 11- FTIR spectra from 600 to 2000 cm^{-1} for PANI-DBSA and PANI/SBS blends with 40 wt% of PANI and different SBS contents (from 40 to 55 wt%). The typical Benzenoid (B) and Quinoid (Q) bands of PANI and the polystyrene and polybutadiene bands of SBS are identified.

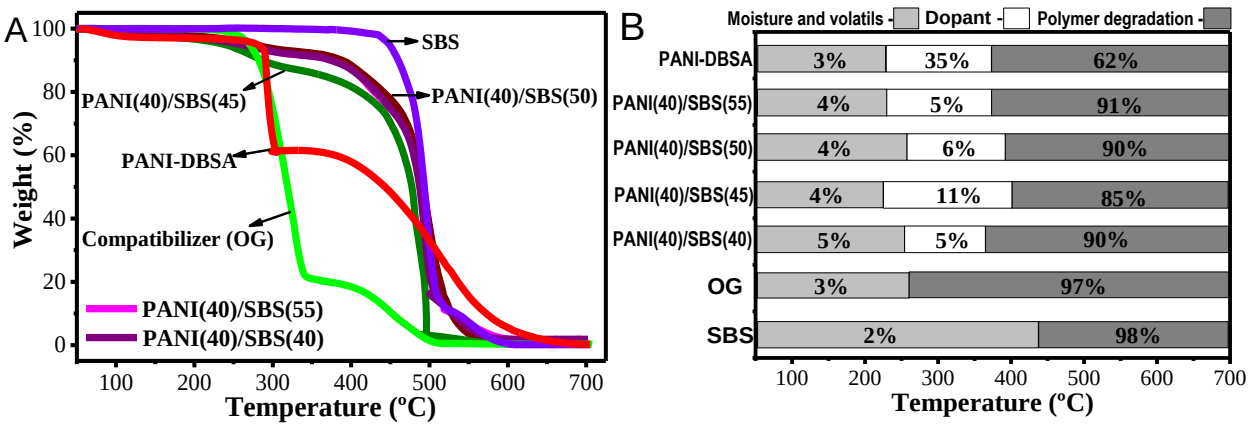

Figure 12- A) Thermogravimetric analysis of PANI-DBSA, OG, SBS and several PANI/SBS blends with varying the SBS contents from 40 to 55 wt%. Measurements performed at 10 °C/min. B) Temperature intervals with corresponding weight losses for the different degradation (Moisture and volatiles, dopant and polymer degradation) events of different samples.

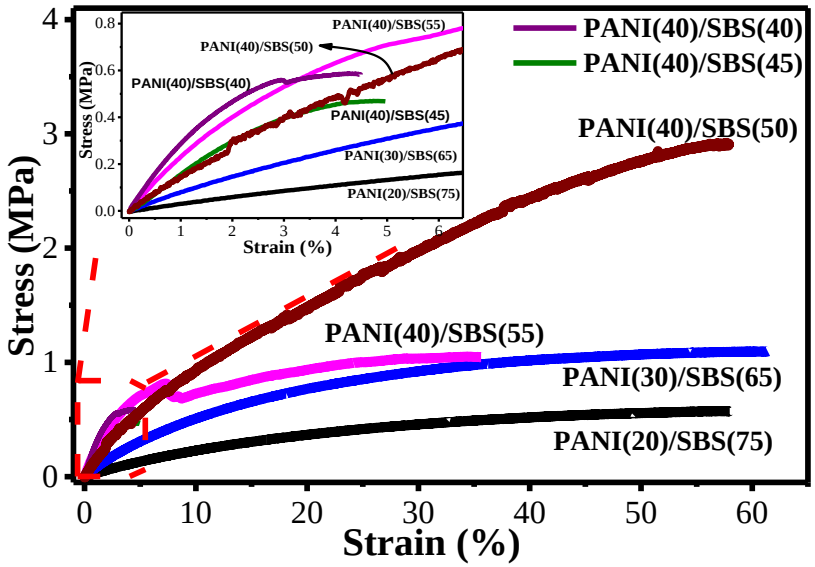

Figure 13- Stress-strain behavior of several PANI/SBS blends until rupture at deformation rates of 1 mm/min. The PANI content varies from 20 to 40 wt% and the SBS content from 40 to 75 wt%, ranging the OG from 5 to 20 wt%.

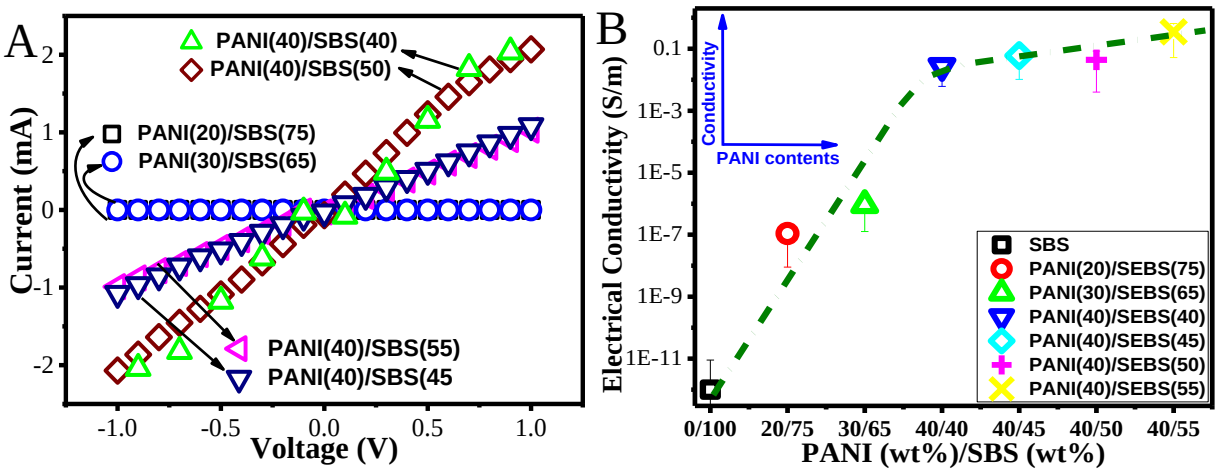

Figure 14- Electrical properties of the PANI/SBS blends with A) I-V curves between -1 to +1 V and B) conductivity of the PANI/SBS blends until 40 wt% PANI. The electrical percolation threshold is around 20-30 wt% of PANI in the blends. The line in B) is for guiding the eyes.

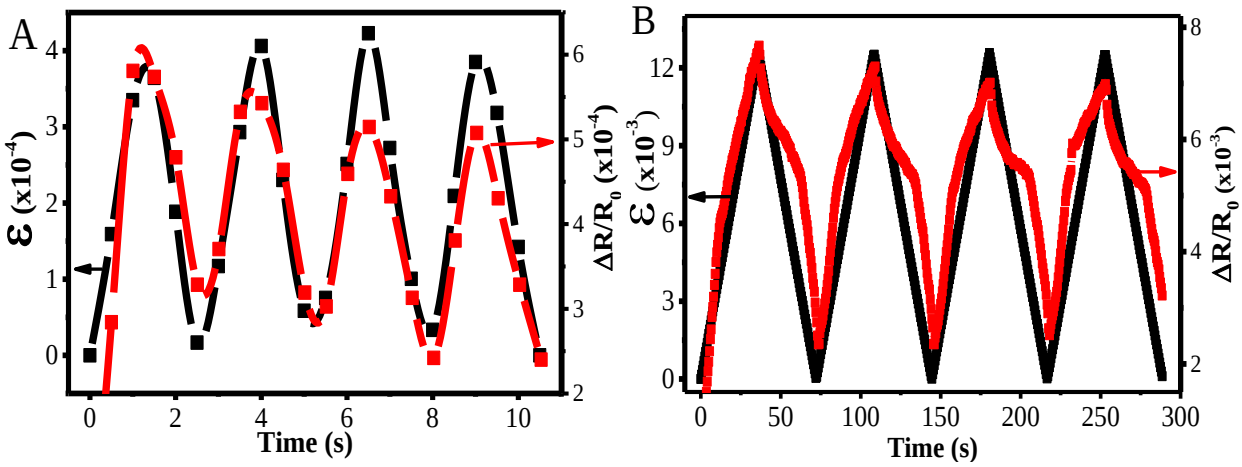

Figure 15- Piezoresistive response of PANI(40)/SBS(55) blends for A) 0.1 and B) 3 mm of deformation in 4-point-bending experiments. The electrical resistance variation follows the mechanical stimulus applied to the blends the different deformations.

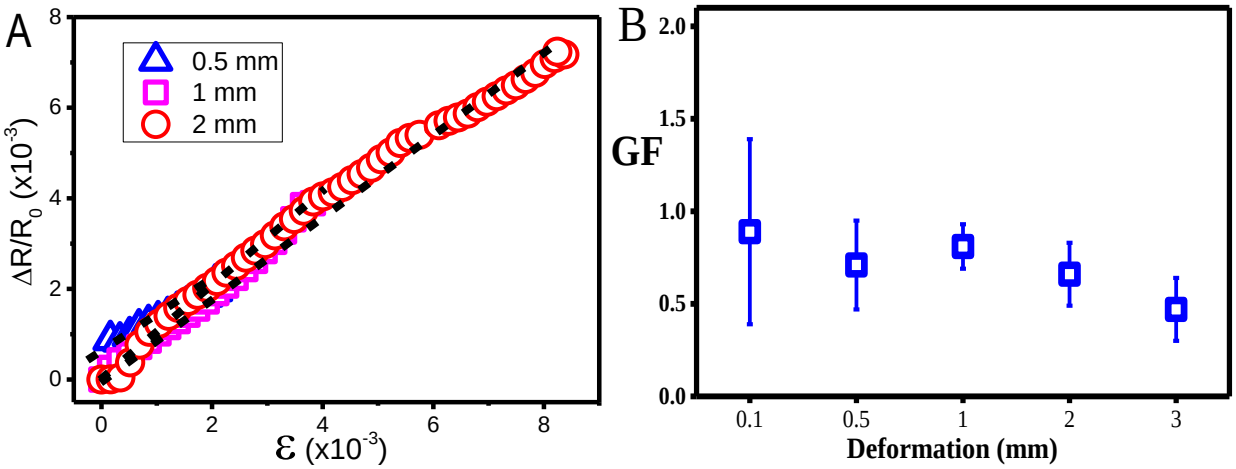

Figure 16- Piezoresistive sensitivity of the PANI/SBS blend with 40 wt% PANI and 55 wt% SBS) in 4-point-bending experiments from 0.1 to 3 mm of deformation. A) Determination of the Gauge Factor (GF) in each deformation cycle and B) GF as function of the applied maximum deformation.

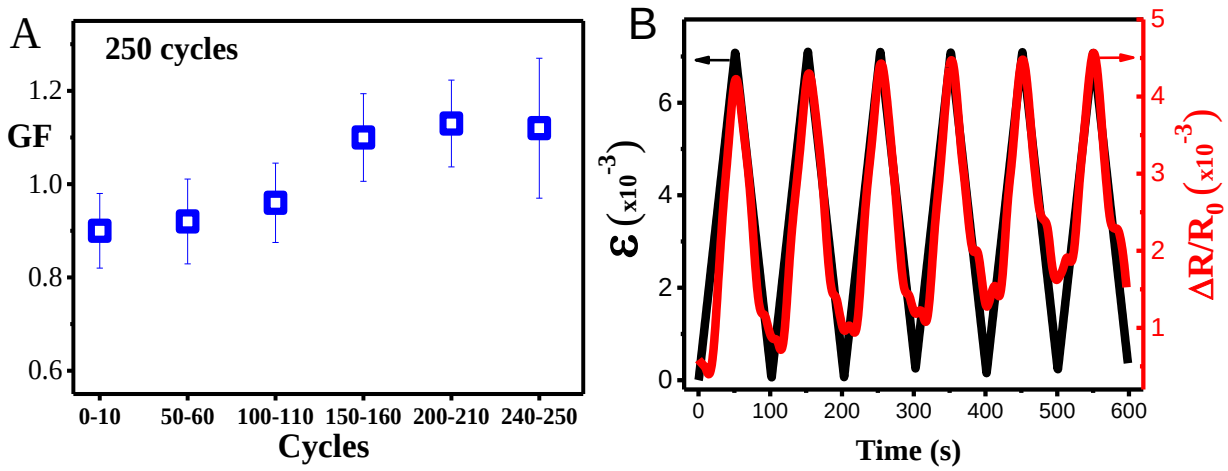

Figure 17- Piezoresistive sensitivity (GF) of the PANI/SBS blend with 40 wt% PANI and 55 wt% SBS, in 4-point-bending measures as a function of the number of cycles (A) Piezoresistive response in temperature, at 40 ºC (B).

Tables

Table 1- Nomenclature of the PANI/SBS blends.

PANI/SBS blend	Sample
20 wt% PANI/5 wt% OG/75 wt% SBS	PANI(20)/SBS(75)
30 wt% PANI/5 wt% OG/65 wt% SBS	PANI(30)/SBS(65)
40 wt% PANI/5 wt% OG/55 wt% SBS	PANI(40)/SBS(55)
40 wt% PANI/10 wt% OG/50 wt% SBS	PANI(40)/SBS(50)
40 wt% PANI/ 15 wt% OG/45 wt% SBS	PANI(40)/SBS(45)
40 wt% PANI/20 wt% OG/40 wt% SBS	PANI(40)/SBS(40)

Table 2- Main mechanical properties of the several extruded PANI/SBS blends.

Sample	Young Modulus (MPa)	Rupture Stress (%)	Rupture Strain (%)
PANI(40)/SBS(40)	30.5 ± 1.5	0.6 ± 0.1	4.4 ± 0.6
PANI(40)/SBS(45)	16.1 ± 0.5	0.5 ± 0.1	5.0 ± 0.7
PANI(40)/SBS(50)	15.0 ± 1.1	2.9 ± 0.2	57.9 ± 5
PANI(40)/SBS(55)	17.3 ± 1.0	1.1 ± 0.1	35.6 ± 4
PANI(30)/SBS(65)	7.7 ± 0.4	1.1 ± 0.1	61.4 ± 5
PANI(20)/SBS(75)	3.1 ± 0.16	0.6 ± 0.1	58.0 ± 4